The total electronic energy change (ΔE) for any of the processes defined in Table 1 contains kinetic (ΔT), electron–electron (ΔV_{ee}), nuclear–nuclear (ΔV_{nn}) and nuclear–electron (ΔV_{ne}) potential energy terms: $\Delta E = \Delta T + \Delta V_{ee} + \Delta V_{nn} + \Delta V_{ne}$. Only the attractive nuclear–electronic potential (ΔV_{ne}) is involved in hyperconjugative interactions. These have been broken down according to molecular orbital symmetry classes. Coulomb repulsions are contained in both ΔV_{ee} and ΔV_{nn}.

Received 22 September 2000; accepted 29 March 2001.

1. Jones, M. Jr *Organic Chemistry* (W. W. Norton & Company, New York, 2000).
2. Carey, F. A. *Organic Chemistry* (McGraw Hill, New York, 2000).
3. McMurry, J. *Organic Chemistry* (Brooks/Cole, Thomson Learning, New York, 1999).
4. Vollhardt, K. P. C. & Schore, N. E. *Organic Chemistry: Structure and Function* (W. H. Freeman and Company, New York, 1998).
5. March, J. *Advanced Organic Chemistry* (John Wiley & Sons, New York, 1992).
6. Loudon, G. M. *Organic Chemistry* (Benjamin/Cummings, Menlo Park, California, 1988).
7. Carey, F. A. & Sundberg, R. J. *Advanced Organic Chemistry* (Kluwer Academic/Plenum, New York, 2000).
8. Sovers, O. J., Kern, C. W., Pitzer, R. M. & Karplus, M. Bond-function analysis of rotational barriers: ethane. *J. Chem. Phys.* **49,** 2592–2599 (1968).
9. Christiansen, P. A. & Palke, W. E. A study of the ethane internal rotation barrier. *Chem. Phys. Lett.* **31,** 462–466 (1975).
10. Bader, R. F. W., Cheeseman, J. R., Laidig, K. E., Wiberg, K. B. & Breneman, C. Origin of rotation and inversion barriers. *J. Am. Chem. Soc.* **112,** 6530–6536 (1990).
11. Brunck, T. K. & Weinhold, F. Quantum mechanical studies on the origin of barriers to internal rotation about single bonds. *J. Am. Chem. Soc.* **101,** 1700–1709 (1979).
12. Reed, A. E. & Weinhold, F. Natural bond orbital analysis of internal rotation barriers and related phenomena. *Isr. J. Chem.* **31,** 277–285 (1991).
13. Wiberg, K. B. & Rablen, P. R. Comparison of atomic charges derived via different procedures. *J. Comp. Chem.* **14,** 1504–1518 (1993).
14. Reed, A. E. & Weinhold, F. Some remarks on the C-H bond dipole moment. *J. Chem. Phys.* **84,** 2428–2430 (1986).
15. Badenhoop, J. K. & Weinhold, F. Natural steric analysis of internal rotation barriers. *Int. J. Quant. Chem.* **72,** 269–280 (1999).
16. Goodman, L., Gu, H. & Pophristic, V. Flexing analysis of ethane internal rotation energetics. *J. Chem. Phys.* **110,** 4268–4275 (1999).
17. Weinhold, F. in *The Encyclopedia of Computational Chemistry* (ed. Schleyer, P. v. R.) 1792–1811 (John Wiley & Sons, Chichester, 1998).
18. Weisskopf, V. F. Of atoms, mountains, and stars: a study in qualitative physics. *Science* **187,** 605–612 (1975).
19. Badenhoop, J. K. & Weinhold, F. Natural bond orbital analysis of steric interactions. *J. Chem. Phys.* **107,** 5406–5421 (1997).
20. Glendening, E. D., Badenhoop, J. K., Reed, A. E., Carpenter, J. E. & Weinhold, F. NBO 4.0 (Theoretical Chemistry Institute, University of Wisconsin, Madison, 1996).
21. Frisch, M. J. *et al.* Gaussian 98 (Gaussian, Pittsburgh, Pennsylvania, 1998).

Acknowledgements

We thank R. Sauers for comments. Support by the National Science Foundation is acknowledged.

Correspondence and requests for materials should be addressed to L.G. (e-mail: goodman@rutchem.rutgers.edu).

Possible displacement of the climate signal in ancient ice by premelting and anomalous diffusion

A. W. Rempel*, E. D. Waddington†, J. S. Wettlaufer*‡ & M. G. Worster§

* *Applied Physics Laboratory, University of Washington, Box 355640, Seattle, Washington 98105, USA*
† *Department of Earth and Space Sciences, University of Washington, Seattle, Washington 98195, USA*
‡ *Department of Physics, University of Washington, Box 351560, Seattle, Washington 98105, USA*
§ *Institute of Theoretical Geophysics, Department of Applied Mathematics and Theoretical Physics, University of Cambridge, Silver Street, Cambridge CB3 9EW, UK*

The best high-resolution records of climate over the past few hundred millennia are derived from ice cores retrieved from Greenland and Antarctica[1–3]. The interpretation of these records relies on the assumption that the trace constituents used as proxies for past climate have undergone only modest post-depositional migration. Many of the constituents are soluble impurities found principally in unfrozen liquid that separates the grain boundaries in ice sheets. This phase behaviour, termed premelting, is characteristic of polycrystalline material[4,5]. Here we show that premelting influences compositional diffusion in a manner that causes the advection of impurity anomalies towards warmer regions while maintaining their spatial integrity. Notwithstanding chemical reactions that might fix certain species against this prevailing transport, we find that—under conditions that resemble those encountered in the Eemian interglacial ice of central Greenland (from about 125,000 to 115,000 years ago)—impurity fluctuations may be separated from ice of the same age by as much as 50 cm. This distance is comparable to the ice thickness of the contested sudden cooling events in Eemian ice from the GRIP core.

At the top of an ice sheet, in the firn layer (typically a few tens of metres thick[6]), some trace constituents are displaced by vapour transport through the connected network of air pockets that

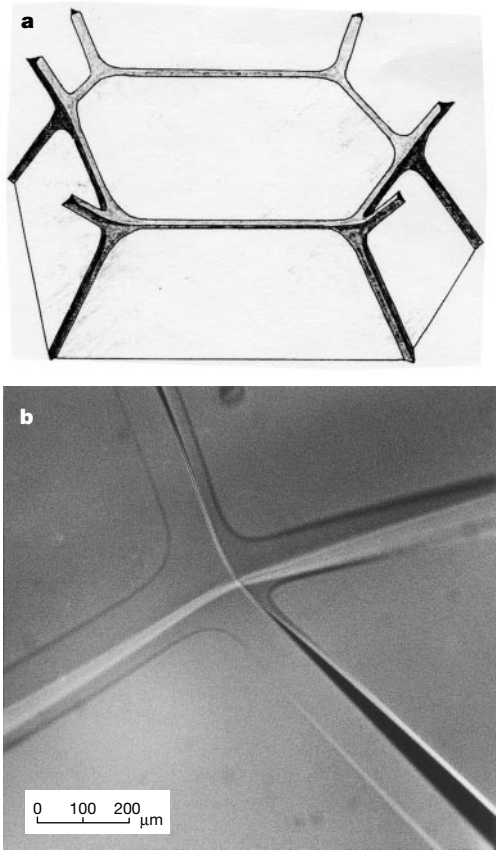

Figure 1 The hydraulic system of polycrystalline ice. **a**, A three-dimensional schematic diagram of the vein–node system (taken from ref. 10, where it was modified from ref. 25). For the dihedral angles observed in ice, the liquid is connected in a continuous network[9]. **b**, A photograph (H. M. Mader, personal communication; see ref. 11) of four veins intersecting at a node between four ice grains near 0 °C. Several mechanisms are responsible for the existence of liquid at temperatures in the solid region of the bulk phase diagram—known as premelting[4,5]—these include the effects of impurities and interfacial curvature, which cause liquid to line the boundaries where three or more grains meet. (Premelted films can form on the surfaces of dust particles, bubbles and clathrate crystals; for typical volume fractions of these constituents, the mass fraction of liquid sequestered in films on their surfaces is expected to be much smaller than the mass fraction of liquid in the vein–node system (see Supplementary Information). Intermolecular interactions between adjacent pairs of grains[4,5] have been invoked to explain laboratory observations of grain-boundary melting[26]; the prevalence of this behaviour in the polar ice sheets has not been measured.)

separate individual ice grains, and seasonal melting can sometimes cause additional advective transport[7]. Beneath the firn, the air pockets are sealed and, at the cold temperatures that prevail within the polar ice sheets, the flow of liquid is likely to be negligible. As solid-state diffusion through single ice grains is extremely slow[8], the impurities are normally considered to be 'frozen' in place. However, the ubiquitous presence of liquid water along the boundaries where three ice grains meet[9] provides an alternative route for diffusive transport. The veins, which separate three adjacent grains, and nodes, which connect the veins at junctions between four grains, form a continuous network of microscopic channels that remain liquid at sub-zero temperatures[9–11] (Fig. 1). Diffusion through the unfrozen liquid within an ice sheet can enhance the exchange of oxygen isotopes[12], present in both the solid and liquid phases, and explains why the amplitude of seasonal variations in the isotopic ratio is reduced much more rapidly than solid-state diffusion can accomplish[13]. Here we model the transport of soluble impurities, which control the fraction of premelted liquid, and explore how records of the bulk concentrations of these climate indicators may have been altered over millennial timescales.

Most impurity molecules are too large to be incorporated within the ice lattice[7]. Instead they are expected to be confined to grain boundaries, either as solid precipitates or, if the temperature is above the eutectic, as dissolved constituents of the liquid phase. At present, the average temperature is roughly −32 °C at the top of the GRIP and GISP2 ice cores in central Greenland[14,15] and −55 °C at Vostok in Antarctica[2]. Even these frigid temperatures are much higher than the eutectic temperatures of some of the aqueous solutions that are likely to be present. For instance, aqueous solutions of sulphuric acid (H_2SO_4), associated with the fallout from volcanic eruptions, have a eutectic temperature of about −73 °C and the eutectic temperature of ammonium hydroxide, tied to periods during which vast continental regions were engulfed in massive forest fires, is roughly −84 °C (ref. 16). Direct evidence for the presence of concentrated acid solutions along the veins in Antarctic ice samples was provided by measurements of sulphur concentrations[17], thought to have derived from H_2SO_4 and the combination of sulphate and nitrate concentrations[18], thought to represent quantities of H_2SO_4 and nitric acid (HNO_3). In order to display the fundamental effect of anomalous diffusion we treat the idealized case in which the liquid contains a single species of dissolved impurities. Because the most prevalent impurity species are often observed to co-vary through large sections of the polar ice sheets, our description of the transport of a single species of dissolved impurities should capture the major features of the transport of the overall chemical signal. Our principal goal is to provide a framework for the future analysis and reanalysis of ice-core chemistry.

The interstitial solute concentration c is the mass of impurity dissolved within a unit mass of the premelted liquid. The value of c at a particular depth is determined by equilibrium requirements, which are imposed by contemporary *in situ* conditions, particularly the temperature. Measurements from ice-core samples yield the

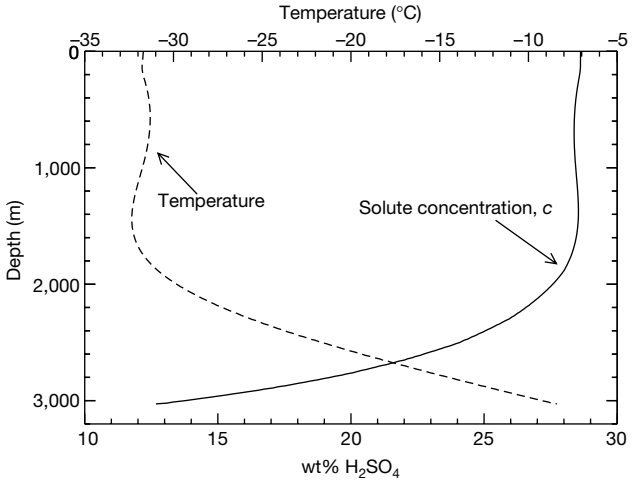

Figure 2 The temperature[14] as a function of depth in the GRIP ice core and the corresponding interstitial concentration of H_2SO_4. At typical ice-core temperatures, the effects of interfacial curvature have a negligible influence on the total liquid fraction in the veins and nodes[10,11], so data from the liquidus relation[16] were used to determine c, after correcting for the pressure dependence of the bulk melting temperature using the Clapeyron equation[19]. For example, ref. 16 states that the liquidus concentration at an undercooling of 29.65 °C and atmospheric pressure is 28% by weight; at an ice-equivalent depth of 2,000 m, the bulk melting temperature is decreased by about 1.3 °C, so we infer that $c \approx 0.28$ when $T \approx -31$ °C at that depth. For comparison, c_B is typically of order 10^{-7} and ϕ is of order 10^{-6}, which is consistent with observations of micrometre-sized veins surrounding grains of a few millimetres in diameter in Antarctic ice[17]. There is empirical evidence to support the assumption, at least for the case of H_2SO_4 (refs 17 and 18), that all the soluble impurities are confined to the liquid, but improved data on the locations of impurities within polycrystalline ice should be acquired. Some researchers have referred to solidification experiments[20] and assumed that most of the impurities are located within the ice grains. The gradual recrystallization of ice grains over thousands of years occurs slowly enough that there seems to be ample justification for assuming that most impurities remain outside the lattice boundaries. The few recognized exceptions to this rule are F^-, Cl^- and NH_3 (ref. 7). Further analysis shows that the essential behaviour reported here does not change significantly when a finite proportion of the impurities resides within the ice lattice because the lattice impurities are expected to equilibrate with the solute in the veins more rapidly than the solute concentration is changed in response to local temperature variations (see Supplementary Information).

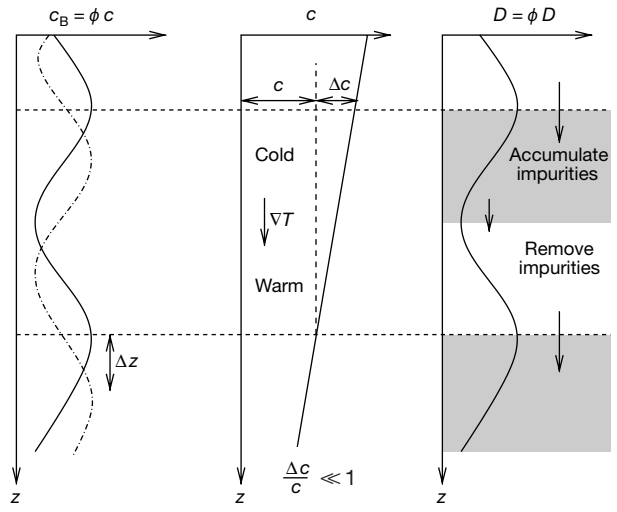

Figure 3 The physical interactions that cause molecular diffusion to alter the c_B-profile in an advective fashion. The left side represents a segment of the c_B-profile that encompasses several annual layers of ice—typically a few centimetres thickness. The corresponding interstitial solute concentration profile $c(z)$ is shown next to this; the temperature contrast across the segment is typically less than 0.01 °C so the associated relative change $\Delta c/c$ is small. Hence, the variation in ϕ mirrors the variation in c_B, as does the effective diffusivity $\bar{D} \equiv \phi D$. The arrows on the right indicate that the rate of diffusive solute transport $\bar{D}\nabla c$ is fastest (slowest) where c_B is greatest (smallest). Impurities accumulate and c_B increases in the shaded region, as the rate of transport into that region is greater than the rate of transport out. (In normal diffusion there is no zone of accumulation.) Variations in the transport rate are 90° out-of-phase with variations in the rate of impurity accumulation; this is a characteristic of wave-like behaviour. The solute concentration is fixed by the thermal field, but ϕ adjusts so that the peaks and troughs in the c_B-profile are translated relative to the ice matrix. After a time Δt the bulk concentration profile has moved a distance of $\Delta z = \mathbf{v}_c \Delta t$ with its shape unaltered, as shown by the dot-dashed line on the left.

bulk impurity concentration c_B, defined as the mass of impurity contained within a unit mass of the polycrystalline sample. Past climate changes are associated with temporal variations in the rate of impurity deposition so that the value of c_B is often observed to double over a distance of a few centimetres, even in ice that is over 100 kyr old. The *in situ* temperature profile is independent of c_B, however, so the liquidus relation indicates that c experiences far more gradual changes with depth (Fig. 2). The conservation of solute requires that $c_B = \phi c$, where ϕ is the mass fraction of liquid. Because c is relatively constant over short distances, the measured centimetre-scale variations in c_B are mirrored by commensurate fluctuations in ϕ. The solute conservation condition employed in our model predicts that, as the surface energy of curved interfaces acts to make vein radii uniform[10,11], variations in c_B must correlate with changes in the total length of veins per unit sample volume. This is confirmed by the observed anti-correlation between c_B and grain size[21,29,30].

We are interested in the movement of impurities relative to the ice matrix, which itself moves downward at velocity $\mathbf{v}$ under the influence of gravity. The ice is approximately incompressible and the velocity of the liquid relative to the ice matrix is small, so we can express the solute balance as

$$\frac{\partial(\phi c)}{\partial t} + \mathbf{v}\cdot\nabla(\phi c) = \nabla\cdot(\phi D\nabla c) \qquad (1)$$

where D is the diffusion coefficient through the liquid. The left side of equation (1) is the rate of change of the mass of impurity within a volume element that moves with the ice matrix at velocity $\mathbf{v}$. The right side represents the effects of molecular (Fickian) diffusion, which are characterized by the effective diffusivity $\tilde{D} \equiv \phi D$. Equation (1) can be written in terms of c_B as

$$\frac{\partial c_B}{\partial t} = -(\mathbf{v} + \mathbf{v}_c)\cdot\nabla c_B - (\nabla\cdot\mathbf{v}_c)c_B \qquad (2)$$

where

$$\mathbf{v}_c \equiv -\frac{D}{c}\nabla c \qquad (3)$$

Moreover, because variations in c_B occur over centimetre-length scales, while variations in $\mathbf{v}_c$ are tied to temperature variations that have characteristic length scales of hundreds of metres, the second (damping) term on the right side of equation (2), involving the divergence of $\mathbf{v}_c$, can be neglected in comparison to the first (advective) term, involving the gradient in c_B (see the Supplementary Information). Equation (2) indicates that, while the ice moves with velocity $\mathbf{v}$, the climate signals contained in the c_B-profile move at a rate that is enhanced by the anomalous velocity $\mathbf{v}_c$. The diffusion of impurities through the liquid alters the c_B-profile in an advective fashion, transporting anomalies in c_B down the solute concentration gradient towards higher temperatures (Fig. 3; see legend for a more detailed explanation of the mechanisms). This transport occurs without significantly altering the amplitudes of the c_B anomalies. This could lead to the misinterpretation of older palaeoclimatic records, which, consistent with the predictions of equation (2), have not undergone the characteristic smoothing that is normally associated with compositional diffusion.

The dashed curve in Fig. 4 shows the magnitude of $\mathbf{v}_c$ as a function of depth for conditions representative of those encountered within the Summit ice cores in Greenland. The anomalous velocity is slow through most of the ice, which is encouraging for the preservation of a consistent age–depth relationship for the long-term averages, measured at the scale of the core bags (55 cm at GRIP), both of soluble constituents that diffuse through the liquid and of palaeoclimatic data that originate from species that move with the local ice velocity. Over tens of thousands of years, however, the motion of the c_B-profile could cause confusion in interpreting the relative timing of palaeoclimatic anomalies. This is illustrated by the solid curve in Fig. 4, which shows a conservative estimate of the separation between the c_B-profile and ice of the same age. At a depth of 2,800 m, which corresponds to the Eemian age in the Summit ice cores, the isochrones are separated by about 50 cm—this is comparable to the thickness of the ice layers that correspond to the sudden cooling events detected in the Eemian ices from the GRIP core, stressing the need for higher-resolution ice-core chemical records.

In order to illuminate the underlying physics of anomalous diffusion, we have presented a simple model based on fundamental mechanisms. In actual ice sheets there are always many species of soluble impurities present in the premelted liquid, and equilibrium with the solid grains is achieved by adjusting ϕ in response to variations in both temperature and solution chemistry. This implies that the variation in c for a particular impurity is not necessarily monotonic in T, and that $\mathbf{v}_c$ varies between different species. In addition, some impurities precipitate onto the grain boundaries at colder temperatures and dissolve only toward the base of the ice sheet, where warmer temperatures make them stable in solution. A more complete understanding of the phase relationships and chemical interactions between the various impurity species is needed before these known effects can be incorporated into predictive models. Chemical interactions might explain why the c_B anomalies are still in the Eemian isotopic events[22], for instance, though these observations could also be explained by the hypothesis that the ice stratigraphy has been disrupted[23] in the recent past. The model presented here should be regarded as a test of the potential for diffusion in the unfrozen liquid to disrupt palaeoclimatic records and a challenge to motivate further high-resolution examinations of the deep ice cores. For example, our predictions indicate

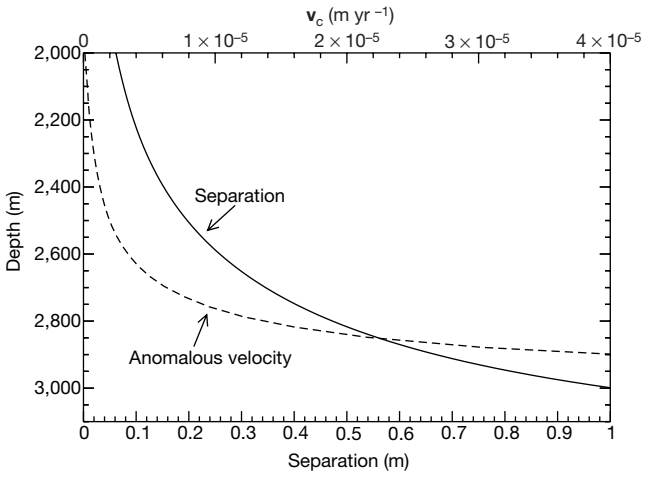

Figure 4 Anomalous diffusion of H_2SO_4 under conditions found at Summit, Greenland. We focus on the bottom portion of the ice sheet where the decrease in c (Fig. 2) causes $\mathbf{v}_c$ to become significant (see equation (3)). The dashed curve shows $|\mathbf{v}_c|$ as a function of depth when the contemporary temperature field at GRIP is used to infer the dependence of c on depth. For solute transport through the veins of polycrystalline ice, D is reduced to one-third the normal molecular diffusivity when the veins are randomly oriented with respect to the concentration gradient[10]; as a lower bound we take $D \approx 5 \times 10^{-10}$ m^2 s^{-1} (ref. 16). The solid curve shows the separation between the c_B-profile and ice of the same age. We used a steady-state Dansgaard–Johnsen[27] flow model for the ice with a kink point at 600 m above the base (20% of the 3,000-m ice thickness) and an accumulation rate of 0.23 m yr^{-1}. Past changes in the temperature profile were investigated using time-dependent heat and mass-flow models; in the depth range shown, these lead to variations in predicted magnitudes of $\mathbf{v}_c$ of up to 30% over the past 100 kyr. Accumulation rates during the last glacial period were lower than today by as much as a factor of four[28] so our steady-state flow model underestimates the age of the ice near the base. As this is where $|\mathbf{v}_c|$ is highest, the data presented here should tend to underestimate the separation between isochrones of the ice and isochrones of the c_B-record.

that anomalous diffusion can displace the sulphuric acid spikes that are used as stratigraphic markers to correlate timescales between different ice cores and the tephra deposits contained in other sedimentary records[24]. Our model explains how diffusion preserves the amplitudes of anomalies in the c_B record, but the anomalies themselves are translated relative to the surrounding ice. Efforts should be made to account for this behaviour when analysing data from the older portions of ice cores by increasing spatial resolution. This could be particularly important when the relative timing of concentration peaks is needed to test theories for the causal links between the various climate proxies. □

Received 2 October 2000; accepted 2 April 2001.

1. Dansgaard, W. *et al.* Evidence for general instability of past climate from a 250-kyr ice-core record. *Nature* **364,** 218–220 (1993).
2. Petit, J. R. *et al.* Climate and atmospheric history of the past 420,000 years from the Vostok ice core, Antarctica. *Nature* **399,** 429–436 (1999).
3. Alley, R. B. Ice-core evidence of abrupt climate changes. *Proc. Natl Acad. Sci. USA* **97,** 1331–1334 (2000).
4. Dash, J. G., Fu, H. Y. & Wettlaufer, J. S. The premelting of ice and its environmental consequences. *Rep. Prog. Phys.* **58,** 115–167 (1995).
5. Wettlaufer, J. S. Ice surfaces: Macroscopic effects of microscopic structure. *Phil. Trans. R. Soc. Lond. A* **357,** 3403–3425 (1999).
6. Paterson, W. S. B. *The Physics of Glaciers* 3rd edn, 8–25 (Pergamon, Oxford, 1994).
7. Wolff, E. W. in *Chemical Exchange Between the Atmosphere and Polar Ice* (eds Wolff, E. W. & Bales, R. C.) 541–560 (NATO ASI Series I, Vol. 43, Springer, Berlin, 1996).
8. Ramseier, R. O. Self-diffusion of tritium in natural and synthetic ice monocrystals. *J. Appl. Phys.* **38,** 2553–2556 (1967).
9. Nye, J. F. in *Physics and Chemistry of Ice* (eds Maeno, N. & Hondoh, T.) 200–205 (Hokkaido Univ. Press, 1992).
10. Nye, J. F. The geometry of water veins and nodes in polycrystalline ice. *J. Glac.* **35,** 17–22 (1989).
11. Mader, H. M. Observations of the water-vein system in polycrystalline ice. *J. Glac.* **38,** 333–347 (1992).
12. Nye, J. F. Diffusion of isotopes in the annual layers of ice sheets. *J. Glac.* **44,** 467–468 (1998).
13. Johnsen, S. J. *et al.* in *Ice Physics and the Natural Environment* (eds Wettlaufer, J. S., Dash, J. G. & Untersteiner, N.) 89–107 (NATO ASI Series I, Vol. 56, Springer, Berlin, 1999).
14. Gundestrup, N. S., Dahl-Jensen, D., Johnsen, S. J. & Rossi, A. Bore-hole survey at dome GRIP—1991. *Cold Reg. Sci. Technol.* **21,** 399–402 (1993).
15. Cuffey, K. M. *et al.* Large Arctic temperature-change at the Wisconsin–Holocene glacial transition. *Science* **270,** 455–458 (1995).
16. Weast, R. C. (ed.) *CRC Handbook of Chemistry and Physics* 68th edn, D219–D269 (CRC Press, Boca Raton, 1987).
17. Mulvaney, R., Wolff, E. W. & Oates, K. Sulphuric acid at grain-boundaries in Antarctic ice. *Nature* **331,** 247–249 (1988).
18. Fukazawa, H., Sugiyama, K., Mae, S. J., Narita, H. & Hondoh, T. Acid ions at triple junction of Antarctic ice observed by Raman scattering. *Geophys. Res. Lett.* **25,** 2845–2848 (1998).
19. Wood, S. E. & Battino, R. *Thermodynamics of Chemical Systems* (Cambridge Univ. Press, Cambridge, 1990).
20. Gross, G. W., Chen-ho, W., Bryant, L. & McKee, C. Concentration dependent solute redistribution at the ice/water phase boundary. II. Experimental investigation. *J. Chem. Phys.* **62,** 3085–3092 (1975).
21. Thorsteinsson, T., Kipfstuhl, J., Eicken, H., Johnsen, S. J. & Fuhrer, K. Crystal size variations in Eemian-age ice from the GRIP ice core, central Greenland. *Earth Planet. Sci. Lett.* **131,** 381–394 (1995).
22. Steffensen, J. P., Clausen, H. B., Hammer, C. U., Legrand, M. & De Angelis, M. The chemical composition of cold events within the Eemian section of the Greenland Ice Core Project ice core from Summit. *J. Geophys. Res.* **102,** 26747–26754 (1997).
23. Alley, R. B. *et al.* Comparison of deep ice cores. *Nature* **373,** 393–394 (1995).
24. Zielinski, G. A. Use of paleo-records in determining variability within the volcanism-climate system. *Quat. Sci. Rev.* **19,** 417–438 (2000).
25. Smith, C. S. Grains, phases and interfaces: An introduction to microstructure. *Trans. Metall. Soc. AIME* **175,** 15–51 (1948).
26. Ohtomo, M. & Wakahama, G. Growth-rate of recrystallization in ice. *J. Phys. Chem.* **87,** 4139–4142 (1983).
27. Dansgaard, W. & Johnsen, S. J. A flow model and a time scale for the ice core from Camp Century, Greenland. *J. Glac.* **8,** 215–223 (1969).
28. Cuffey, K. M. & Clow, G. D. Temperature, accumulation, and ice sheet elevation in central Greenland through the last deglacial transition. *J. Geophys. Res.* **102,** 26383–26396 (1997).
29. Thorsteinsson, T., Kipfstuhl, J. & Miller, H. Textures and fabrics in the GRIP ice core. *J. Geophys. Res.* **102,** 26583–26599 (1997).
30. De la Chapelle, S., Castelnau, O., Lipenkov, V. & Duval, P. Dynamic recrystallization and texture development in ice as revealed by the study of deep ice cores in Antarctica and Greenland. *J. Geophys. Res.* **103,** 5091–5105 (1998).

Supplementary information is available from *Nature*'s World-Wide Web site (http://www.nature.com) or as paper copy from the London editorial office of *Nature*.

Acknowledgements

We acknowledge R. Alley, J. G. Dash, D. P. Winebrenner, S. G. Warren, G. W. Gross, S. F. Johnsen, J. F. Nye, E. J. Steig, J. P. Steffensen and E. W. Wolff for discussions that have influenced this work. We also thank H. M. Mader for providing the photograph for Figure 1b. Support for this research has been provided by the US National Science Foundation.

Correspondence and requests for materials should be addressed to A.W.R. (e-mail: awrempel@apl.washington.edu).

The post-spinel transformation in Mg_2SiO_4 and its relation to the 660-km seismic discontinuity

Sang-Heon Shim*, Thomas S. Duffy* & Guoyin Shen†

** Department of Geosciences, Princeton University, Princeton, New Jersey 08544, USA*

† CARS, University of Chicago, Chicago, Illinois 60637, USA

The 660-km seismic discontinuity in the Earth's mantle has long been identified with the transformation of $(Mg,Fe)_2SiO_4$ from γ-spinel (ringwoodite) to $(Mg,Fe)SiO_3$-perovskite and (Mg,Fe)O-magnesiowüstite. This has been based on experimental studies of materials quenched from high pressure and temperature[1–3], which have shown that the transformation is consistent with the seismically observed sharpness and the depth of the discontinuity at expected mantle temperatures[4]. But the first *in situ* examination of this phase transformation in Mg_2SiO_4 using a multi-anvil press[5] indicated that the transformation occurs at a pressure about 2 GPa lower than previously thought (equivalent to ~600 km depth) and hence that it may not be associated with the 660-km discontinuity. Here we report the results of an *in situ* study of Mg_2SiO_4 at pressures of 20–36 GPa using a combination of double-sided laser-heating and synchrotron X-ray diffraction in a diamond-anvil cell. The phase transformation from γ-Mg_2SiO_4 to $MgSiO_3$-perovskite and MgO (periclase) is readily observed in both the forward and reverse directions. In contrast to the *in situ* multi-

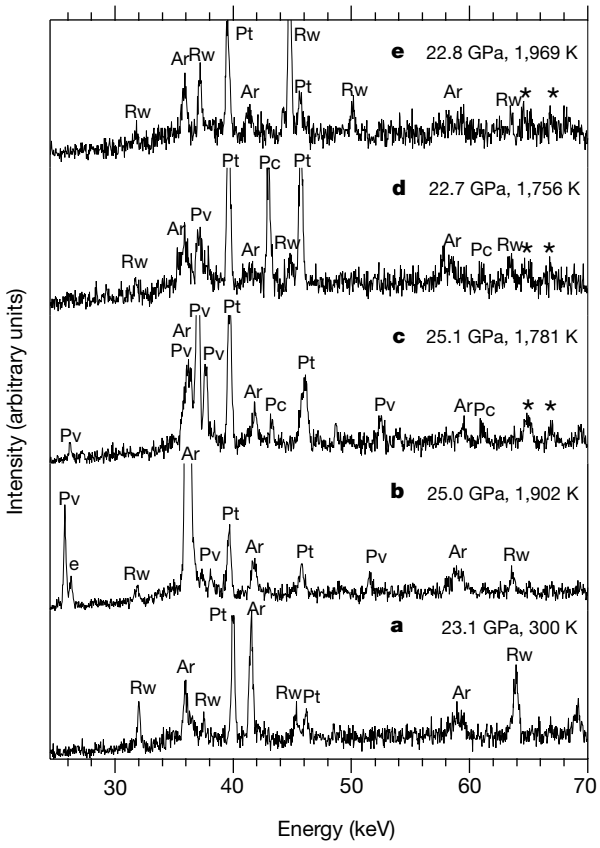

Figure 1 a–e, Representative X-ray diffraction patterns at the indicated *P–T* conditions. Peak identifications are: Rw, ringwoodite; Pv, perovskite; Pc, periclase; Pt, platinum; Ar, argon; asterisk, platinum fluorescence; e, detector escape peak.